



Measurements of stray antenna capacitance in the STEREO/WAVES instrument: Comparison of the radio frequency voltage spectrum with models of the galactic nonthermal continuum spectrum

J. P. Eastwood,¹ S. D. Bale,^{1,2} M. Maksimovic,³ I. Zouganelis,⁴ K. Goetz,⁵ M. L. Kaiser,⁶ and J.-L. Bougeret³

Received 22 January 2009; revised 8 May 2009; accepted 27 May 2009; published 14 August 2009.

[1] The STEREO/WAVES instrument is designed to measure interplanetary radio emission and in situ plasma waves in the solar wind. The instrument uses three orthogonal monopole electric antennas as its sensor system in both a pseudodipole and monopole mode. At high radio frequencies, the capacitance of the antennas determines the system gain. Here we estimate the stray capacitance in the antenna system by comparing the measured voltage spectrum with a model of the galactic continuum spectrum, which is the instrument background at high frequencies. Together with the antenna free-space capacitance, these measurements provide an absolute calibration of the STEREO/WAVES experiment at radio frequencies, a prerequisite for quantitative studies of solar and astrophysical radio emission.

Citation: Eastwood, J. P., S. D. Bale, M. Maksimovic, I. Zouganelis, K. Goetz, M. L. Kaiser, and J.-L. Bougeret (2009), Measurements of stray antenna capacitance in the STEREO/WAVES instrument: Comparison of the radio frequency voltage spectrum with models of the galactic nonthermal continuum spectrum, *Radio Sci.*, 44, RS4012, doi:10.1029/2009RS004146.

1. Introduction

[2] STEREO is a two spacecraft mission designed to study the causes, mechanisms and dynamics of coronal mass ejections (CMEs), the locations and nature of particle acceleration in the solar wind and corona, and the structure of the solar wind as a whole [Kaiser *et al.*, 2008]. To achieve these goals, each STEREO spacecraft carries an identical suite of instruments capable of making both remote and in situ measurements. An important component of this instrument suite is the STEREO/WAVES (S/WAVES) radio experiment [Bougeret *et al.*,

2008]; both CMEs and flares generate radio emission that can be used to remotely track and probe plasma dynamics in the corona and solar wind. CMEs generate so-called type II radio bursts; as they propagate into the heliosphere they drive strong interplanetary (IP) shocks, which in turn energize solar wind electrons to form upstream propagating electron beams. These electron beams generate plasma radio emission at the electron plasma frequency f_{pe} and its harmonic $2f_{pe}$ ahead of the shock. Type III bursts are produced by energetic electron beams injected by flares onto open magnetic field lines. By combining the two spacecraft measurements with direction finding ('goniopolarimetry'), it is possible to pinpoint the location of the radio emission in space, and track its movement with time [Cecconi *et al.*, 2008].

[3] S/WAVES uses three 6-m monopole antennas, orthogonally mounted on the spacecraft, to measure the electric field of both free electromagnetic and plasma wave fluctuations. The antenna system is described in detail by Bale *et al.* [2008]. Since the ambient plasma density falls with distance from the Sun, both type II and type III radio emission exhibit a characteristic drift from high to low frequency. To accommodate this, the signal is processed by a variety of receivers, each covering a

¹Space Sciences Laboratory, University of California, Berkeley, California, USA.

²Department of Physics, University of California, Berkeley, California, USA.

³LESIA, Section Meudon, Observatoire de Paris, Meudon, France.

⁴Laboratoire de Physique des Plasmas, UPMC, Ecole Polytechnique, CNRS, Saint-Maur-des-Fossés, France.

⁵School of Physics and Astronomy, University of Minnesota, Minneapolis, Minnesota, USA.

⁶NASA Goddard Space Flight Center, Greenbelt, Maryland, USA.

different frequency range [Bougeret *et al.*, 2008]. The Low-Frequency Receiver (LFR) covers the frequency range 2.5–160 kHz, the High-Frequency Receiver (HFR) covers 125 kHz to 16.025 MHz, and the Fixed Frequency Receiver (FFR) operates at either 30.025 or 32.025 MHz. The instrument is also capable of capturing time series of data to study local langmuir waves and measure the plasma density. Here we examine in detail the High-Frequency Receiver; the HFR frequency range covers radio emission generated from a few solar radii to approximately 0.5 AU from the Sun [Bougeret *et al.*, 2008] and is particularly relevant for studies of type II and type III emission.

[4] The HFR returns data in two channels. Each channel is connected to a different combination of the monopoles. For example, in a typical operating mode, the HFR channel 1 data is based on the dipole created by the E_x and E_y antennas, and the HFR channel 2 data is based on the E_z monopole antenna. Data from the two channels are also cross-correlated; the cross-correlated signal is necessary for the direction finding techniques. HFR data are first available in terms of the measured voltage power P_{meas} (V^2Hz^{-1}). They have already been calibrated to the extent that the raw telemetry has been correctly converted into this physical unit (M. Maksimovic, Calibration of flight models 1 and 2 of STEREO/WAVES, LESIA, Meudon, internal report, 2007). However, in order to perform quantitative studies, and relate observations to previous results, it is necessary to further calibrate the data in units of incident flux S ($Wm^{-2}Hz^{-1}$). Generally speaking, this must be done in flight because sources of unwanted radio noise must be identified, the antenna response must be examined and the stray capacitance of the spacecraft must be quantified.

[5] In this paper we examine this problem in detail, and use the results to develop calibration procedures for the S/WAVES experiment. Furthermore, the calibration is benchmarked against independently calibrated data from the WIND spacecraft. The overall analysis procedure is described in section 2. In section 3, the theoretical properties of the frequency-dependent antenna capacitance and antenna effective length are examined. In section 4, sources of unwanted radio noise are identified, and in section 5 the data from both STEREO spacecraft are compared to the galactic nonthermal continuum spectrum; through this comparison the stray capacitance is estimated. The calibrated STEREO data are compared to independently calibrated WIND observations of a Type III radio burst in section 6, and conclusions are presented in section 7.

2. Analysis

[6] The measured power, P_{meas} , consists of several signals. The first, P' , is the signal we are attempting to

measure. The second, P_{sc} , is the noise generated by the preamplifiers, instrument electronics and the spacecraft itself. The third, P_{shot} , is the shot noise generated by the interaction of each antenna with the local plasma.

$$P_{meas} = P' + P_{sc} + P_{shot} \quad (1)$$

[7] However, P' is not equal to the open circuit voltage power collected by the antenna. Stray capacitance reduces the measured signal [Manning, 2000] such that the open circuit power, P , is given by

$$P = \left(\frac{C_A}{C_A + C_{St}} \right)^{-2} P' \quad (2)$$

where C_A is the frequency-dependent capacitance of the antenna and C_{St} is the system stray capacitance. The stray capacitance consists of the base capacitance of the antenna itself, the cable capacitance and the preamplifier input capacitance [Bale *et al.*, 2008]. The open circuit power (P) is related to the incident electromagnetic flux S by

$$S = \frac{\langle E^2 \rangle}{Z_0} = \frac{P}{Z_0 L_{eff}^2} \quad (3)$$

where $Z_0 \approx 120\pi \Omega$ is the impedance of free space and L_{eff} is the ‘effective length’ of the antenna. Combining these equations, we have the following expression:

$$S = \frac{\langle E^2 \rangle}{Z_0} = \frac{1}{Z_0 L_{eff}^2} \left(\frac{C_A}{C_A + C_{St}} \right)^{-2} (P_{meas} - P_{sc} - P_{shot}) \quad (4)$$

$$S = \frac{\langle E^2 \rangle}{Z_0} = \frac{1}{Z_0 L_{eff,c}^2} (P_{meas} - P_{sc} - P_{shot}) \quad (5)$$

[8] In equation (5) the gain $C_A/(C_A + C_{St})$ has been folded into the effective length (here denoted $L_{eff,c}$). It should be noted that the low-frequency limit of $L_{eff,c}$ is sometimes also quoted as the ‘effective length’ [Rucker *et al.*, 1996; Bale *et al.*, 2008].

[9] In summary, the following parameters must be evaluated in order to convert the measured signal P_{meas} (V^2Hz^{-1}) to S ($Wm^{-2}Hz^{-1}$): the antenna capacitance $C_A(f)$, the effective antenna length L_{eff} , the spacecraft generated noise P_{sc} , the antenna shot noise P_{shot} and the stray capacitance C_{St} . In the next section we consider

the antenna capacitance and effective length in more detail.

3. Theoretical Behavior of a Dipole

3.1. Capacitance

[10] A dipole has an impedance Z_D

$$Z_D = 20k^2 \left(\frac{L}{2}\right)^2 - j \frac{120(\ln(L/2a) - 1)}{\tan(kL/2)} \quad (6)$$

where L is the physical length of the dipole (tip to tip), a is the antenna radius, and k is the wave number of the incident electromagnetic wave [Hansen, 1981]. If the dipole antenna is operating in the capacitive regime, then we can compute its capacitance, C_D :

$$\frac{1}{\omega C_D} = \frac{120(\ln(L/2a) - 1)}{\tan(kL/2)} \quad (7)$$

$$C_D = \frac{\epsilon_0 \pi}{k} \frac{\tan(kL/2)}{(\ln(L/2a) - 1)} \quad (8)$$

The dipole capacitance depends on the frequency of the incident wave. In the short dipole regime, at long wavelengths ($\lambda \gg L$), C_D is given by [Manning, 2000; Zarka et al., 2004]:

$$C_D = \frac{\epsilon_0 \pi (L/2)}{(\ln(L/2a) - 1)} \quad (9)$$

We first consider the dipole created by the E_x and E_y monopoles. The physical length of this dipole is 10.4 m (two 6 m antennas separated by an angle of 120°). The mean radius is 0.0115 m. The capacitance of the $E_x - E_y$ dipole in the low-frequency limit is thus ~ 28 pF.

[11] In examining the monopole data, the the monopole capacitance is equivalent to twice that of a dipole with twice its length [Manning, 2000]. Thus the antenna capacitance of the E_z monopole is ~ 62 pF in the low-frequency limit [Bale et al., 2008].

3.2. Resistance and Effective Length

[12] The resistance of the dipole, R_D is given by the real part of equation (6) [Balanis, 2005], and can be written as

$$R_D = 20k^2 \left(\frac{L}{2}\right)^2 = 80 \left(\frac{(L/2)f\pi}{c}\right)^2 \quad (10)$$

where f is the frequency of the incident electromagnetic wave and c is the speed of light. The electric field of the electromagnetic wave E induces a potential difference V across the antenna. Assuming that the directional gain of

the antenna is 1, and that the electric field and the antenna are aligned, V can be expressed as a function of E .

$$V = \sqrt{\frac{R_D}{Z_0 \pi}} \lambda E \quad (11)$$

[13] Substituting the expression for R_D , and rearranging, we find

$$P = \langle V^2 \rangle = \frac{2}{3} Z_0 \left(\frac{L}{2}\right)^2 S \quad (12)$$

where $S = E^2/Z_0$. Comparing equation (12) to equation (3), it can be seen that the effective length of the short dipole is

$$L_{\text{eff}} = \sqrt{\frac{2}{3}} \left(\frac{L}{2}\right) \quad (13)$$

where L is the true length of the dipole. Consequently, the effective length of the $E_x - E_y$ dipole is 4.25 m and the effective length of the E_z monopole is 2.45 m.

4. Sources of Noise

[14] Having determined C_A and L_{eff} from the theoretical properties of the antenna, we now consider the noise present in the measurements. Two main sources must be accounted for. The first is radio frequency noise generated by the spacecraft itself which can be quantified by using data collected during the commissioning of the instrument. The second is shot noise, caused by the interaction of the thermal plasma with the antennas.

4.1. Spacecraft-Generated Noise

[15] Radio frequency noise generated by the spacecraft itself can be determined from data acquired during commissioning. The antennas are stowed before launch, but the receiver is switched on prior to their deployment. The signal measured during this predeployment interval can be used to quantify the spacecraft noise. The S/WAVES experiment on STEREO A was switched on at ~ 1450 UT on 27 October 2006. The first antenna was deployed at 1640 UT. A ~ 10 -min period broadband oscillation in the measured signal was observed in both Channels 1 and 2. The source of this oscillation is unknown. The background signal, averaged over a quiet 5-min interval (1500–1505 UT), is shown in Figure 1a. Note that we have removed all the terrestrial RFI signals from the background measurements. For the majority of the predeployment interval, HFR channel 1 was connected to the $+E_x$ monopole, and HFR channel 2 was connected to the $-E_y$ monopole. Ideally, one should measure the predeployment signal for each possible

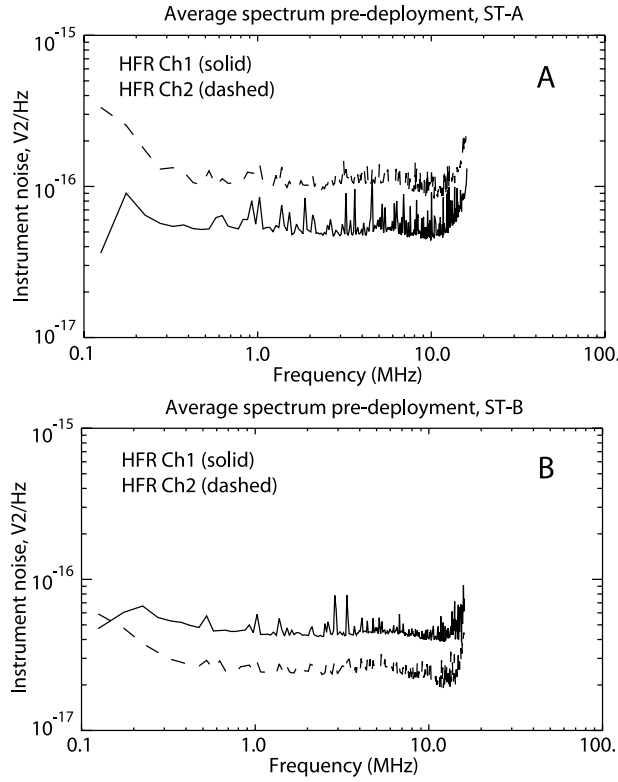


Figure 1. Spacecraft noise on (a) STEREO A and (b) STEREO B as measured by the S/WAVES instrument. The ST-A spectrum is the average observed between 1500 and 1505 UT, 27 October 2006, and the ST-B spectrum is the average observed between 0330 and 0830 UT, 28 October 2006. In both cases, strong RFI lines have been removed.

combination of monopoles and dipoles used by each channel, and use that specific measurement in the calibration of data taken using the same antenna combinations. However, given the available data we are forced to assume that the background signals shown in Figure 1a are not affected by the exact combination of antennas attached to each channel receiver.

[16] The S/WAVES experiment on STEREO B was also switched on on 27 October 2006, but the first antenna was not deployed until 2123 UT on 29 October 2006. The majority of the data were again collected using the $+E_x$ monopole (HFR channel 1) and the $-E_y$ monopole (HFR channel 2). We have averaged 5 h of observations taken on 28 October 2006 0330–0830 UT. The background signal from STEREO B is shown in Figure 1b where again, terrestrial RFI has been removed. The noise levels associated with Channel 1 on each spacecraft ($+E_x$)

are comparable ($P_{sc} \sim 5 \times 10^{-17} \text{V}^2 \text{Hz}^{-1}$), but Channel 2 on STEREO A is noisier ($P_{sc} \sim 10^{-16} \text{V}^2 \text{Hz}^{-1}$) than on STEREO B ($P_{sc} \sim 3 \times 10^{-17} \text{V}^2 \text{Hz}^{-1}$). This has implications for the calibration of Channel 2 on STEREO A against the galaxy, which is discussed in more detail below.

4.2. Shot Noise

[17] Shot noise, caused by the interaction of the thermal plasma with the antennas [Kellogg, 1981; Meyer-Vernet and Perche, 1989] at frequencies above $1/RC$, is thought to be well modeled by a $1/f^2$ power law, and is important at frequencies below about 500 kHz. The shot noise is of secondary importance, and may in certain circumstances be neglected, in the HFR calibration. It is much more important part of the LFR calibration procedure. Here, we fit a $1/f^2$ power law to the bottom three frequencies observed by HFR (0.125 MHz, 0.175 MHz and 0.225 MHz), and subtract the extension of this fit from the observed data.

5. Galactic Background and Measurement of Stray Capacitance

[18] Thus far, we have determined the theoretical properties of the antennas and sources of noise in the measurements. Referring to section 2, the stray capacitance C_{st} must also be evaluated. In this section we examine an interval of data on 13 January 2007, when no discernable solar emission was observed, such that the measured radio emission corresponds to the galactic background, consisting of synchrotron radiation from galactic and extragalactic sources. Using ground and space-based observations, this galactic background flux density (modulated by the effective collecting area of the dipole), S_g , is given by:

$$S_g = \left[I_g f^{-0.52} \left(\frac{1 - e^{-\tau}}{\tau} \right) + I_{eg} f^{-0.8} e^{-\tau} \right] \Omega \eta \quad (14)$$

where $I_g = 2.48 \times 10^{-20} \text{Wm}^{-2} \text{Hz}^{-1}$ (Galactic), $I_{eg} = 1.06 \times 10^{-20} \text{Wm}^{-2} \text{Hz}^{-1}$ (Extragalactic) and $\tau = 5 \times f^{-2.1}$ is the interstellar opacity [Cane, 1979]. Furthermore, f is the frequency in MHz, the dipole beam area $\Omega = 8\pi/3$ and $\eta(f)$ is a geometrical correction factor for the inhomogeneous distribution of radiation on the sky [Zarka et al., 2004; Dulk et al., 2001; Manning and Dulk, 2001]. Here $\eta = 1$ is used.

[19] An alternative emission model based on satellite data alone [Novaco and Brown, 1978] is given by:

$$S_g = [I_{eg} f^{-0.76} e^{-\tau}] \Omega \eta \quad (15)$$

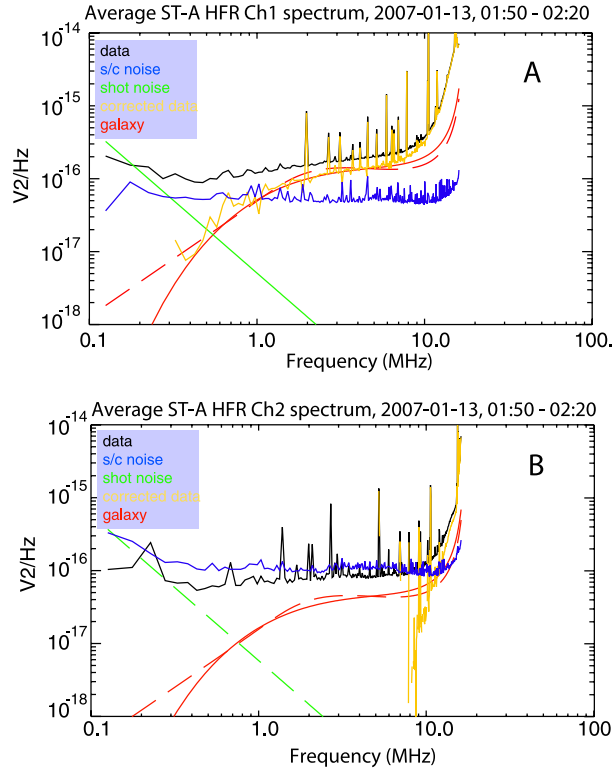


Figure 2. Average spectra for the quiet interval 0150–0220 UT, 13 January 2007 on STEREO A HFR (a) Channel 1 and (b) Channel 2. In each case the black curve is the measured signal, the blue curve is the instrument background, and the green line is the modeled shot noise. The yellow curve is the measured signal with these two sources of noise removed. The dashed and solid red curves correspond to the Cane model and Novaco and Brown model, respectively.

[20] Here $I_{eg} = 1.38 \times 10^{-19} \text{ Wm}^{-2}\text{Hz}^{-1}$ and $\tau = 3.28 \times f^{-0.643}$. On the basis of equation (4),

$$P_g = S_g Z_0 L_{eff}^2 \left(\frac{C_A}{C_A + C_{St}} \right)^2 \quad (16)$$

[21] Thus the galactic signal depends on S_g (see equations (14) and (15)), the effective length L_{eff} , antenna capacitance C_A (see section 3) and the stray capacitance C_{St} . These models are based on observations between 0.1 MHz and >100 MHz, and so are an appropriate reference for the STEREO data.

[22] Figure 2a shows observations from STEREO A HFR channel 1, averaged between 0150 and 0220 UT when no transient (i.e., solar) emission was observed. During this time HFR channel 1 was connected to the

$E_x - E_y$ dipole. The observed signal P_{meas} is shown in black. The blue and green lines show the spacecraft noise P_{sc} and the $1/f^2$ fit to the shot noise P_{shot} . The yellow curve shows P' (see equation (1)): the measured signal with the background and shot noise removed. The increase in the observed power at high frequencies is due to the antenna resonance. Finally, the red lines show the modeled galactic emission P_g , calculated using equation (16) and the Cane model (dashed red line) and the Novaco and Brown model (solid red line). Because of the nonlinear nature of the functions, we performed an iterative fit by inspection until closest agreement was found between P' and P_g . The best agreement between P' and P_g was found to correspond to $C_{St} \sim 40$ pF. The observed resonance peak is broader than that predicted by the model, and there is significant divergence above 10 MHz. The gradient of the observed spectrum is always positive. The Novaco and Brown model appears to better reproduce this shape of the observed spectrum whereas there is an inflection point in the Cane model.

[23] Figure 2b shows similar observations from STEREO A HFR channel 2, which was connected to the E_z monopole. The measured signal (black) and the spacecraft noise (blue) are comparable, except at higher frequencies near the antenna resonance. In fact, below $f = 8$ MHz the measured signal is less than the predeployment noise. The yellow curve shows P' , but it is not resolved over most of the frequency range. Although the red curves show P_g assuming $C_{St} = 70$ pF, the limited knowledge of P' means that this result is not reliable. The fact that the signal observed on 13 January 2007 is less than the signal observed predeployment suggests that the noise was temporarily higher during the commissioning phase. This may be due to the effects of temperature fluctuations during the mission that are currently under investigation. This means that we cannot determine the stray capacitance from the STEREO A monopole data alone, until the nature of the high predeployment noise is better understood.

[24] Figure 3 shows the results from STEREO B in the same format as Figure 2. Figure 3a again shows HFR channel 1, which was similarly connected to the $E_x - E_y$ dipole. P_g requires a stray capacitance ~ 40 pF for the best fit with P' (yellow). Figure 3b shows HFR channel 2, which was connected to the E_z monopole. As seen in Figure 1, the spacecraft noise in channel 2 on STEREO B is lower than on STEREO A, and so the galactic signal can be resolved over the whole frequency range. To appropriately fit the measured signal, $C_{St} \sim 90$ pF.

[25] The stray capacitance of the dipole is half that of the monopole, since $1/C_{St,D} = 1/C_{St,M} + 1/C_{St,M}$. Therefore, from these results we deduce the stray capacitance of each antenna unit to be ~ 80 – 90 pF. This means that the antenna gain $G = 0.4$ – 0.45 . We note that values of

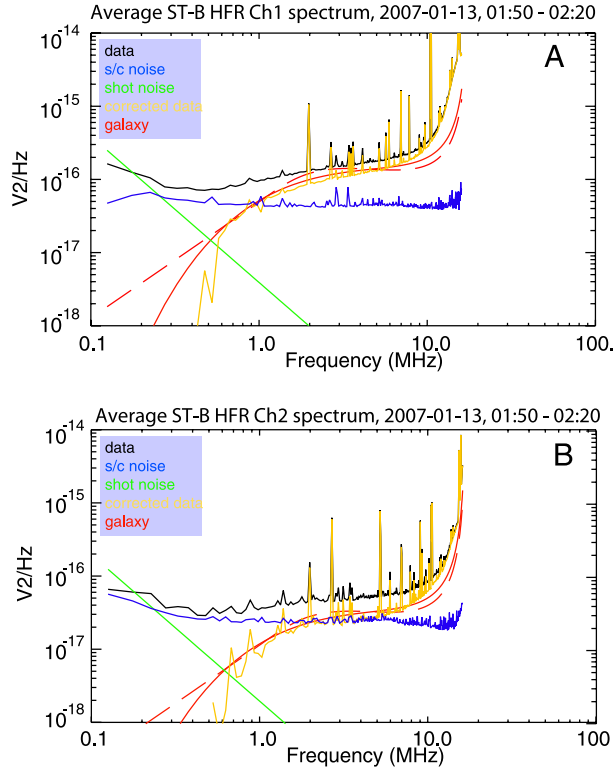


Figure 3. Average spectra for the quiet interval 0150–0220 UT, 13 January 2007 on STEREO B. Figure 3 is in the same format as Figure 2. (a) HFR Channel 1 measurements and (b) HFR Channel 2 measurements. In each case the black curve is the measured signal, the blue curve is the instrument background, and the green line is the modeled shot noise. The yellow curve is the measured signal with these two sources of noise removed. The dashed and solid red curves correspond to the Cane model and Novaco and Brown model, respectively.

stray capacitance estimated from laboratory experiments on flight spare equipment [Bale *et al.*, 2008] are slightly smaller, but still comparable to, the values presented here. In a separate analysis using a very different technique based on measurements of the shot noise (which depends on the antenna impedance), it has been found that the stray capacitance of the $E_x - E_y$ dipole on STEREO B is 32 ± 4 pF (I. Zouganelis *et al.*, Measurements of stray antenna capacitance in the STEREO/WAVES instrument: Comparison of the radio voltage spectrum with the modeled electron shot noise collected on the antennas, submitted to *Radio Science*, 2009). Again, this value is slightly smaller, but comparable to the results here. The antenna properties have also been studied using numerical methods and laboratory rheom-

etry experiments [Oswald *et al.*, 2009], with the aim of understanding in particular the effective directions of the antennas. This analysis requires knowledge of the base capacitance, and the values used are consistent with those found here.

6. Observations of a Type III Burst Observed by STEREO and Wind: Absolute Flux Measurements

6.1. STEREO Observations

[26] Having established the appropriate free parameters, we can now use equation (4) to convert the measured signal P_{meas} into units of incident flux S . As an example, Figure 4 shows STEREO A (Figures 4a and 4b) and STEREO B (Figures 4c and 4d) observations of a Type III radio burst on 16 November 2006. Observations between 200 kHz and 2 MHz are shown on a magnified scale so that the structure of the burst is

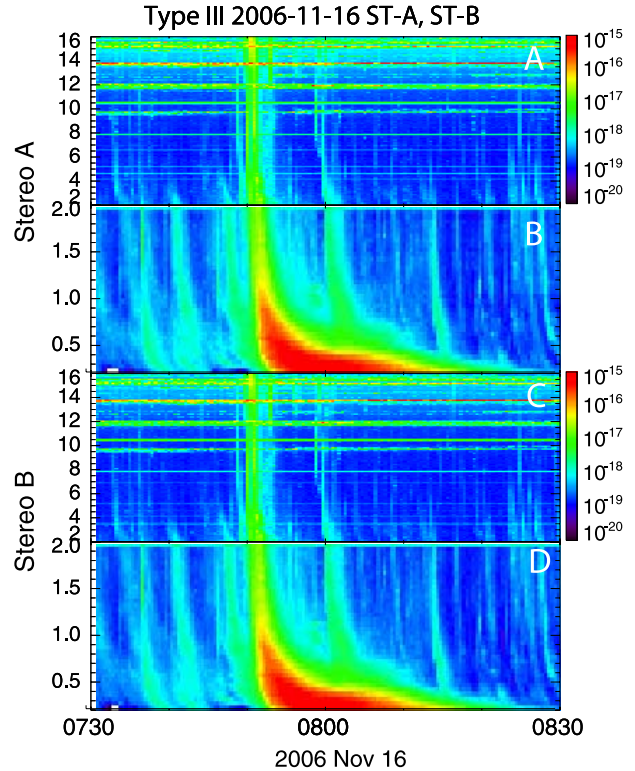


Figure 4. A type III solar radio burst observed by STEREO A and B on 16 November 2006. (a and b) The calibrated Stereo A data and (c and d) the calibrated Stereo B data. Emission at fixed frequency lines corresponds to terrestrial RFI and could be removed in further processing.

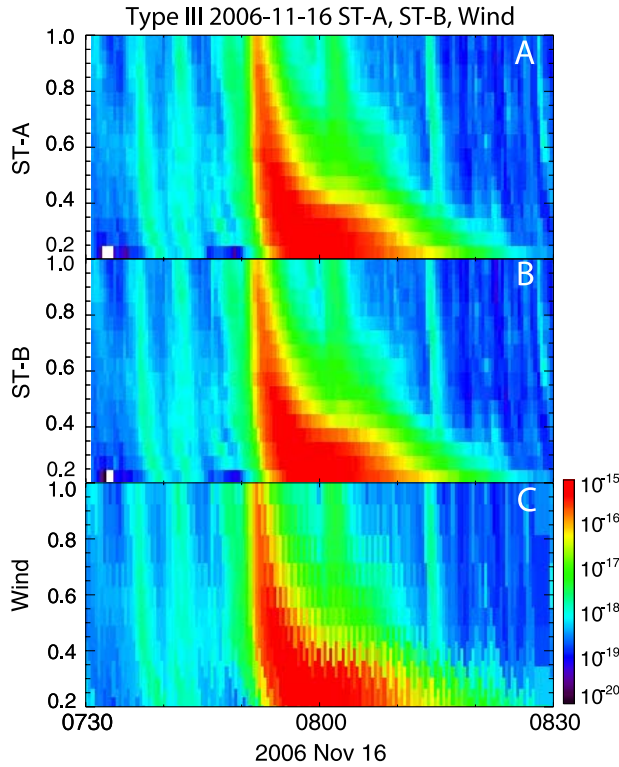


Figure 5. Comparison between independently calibrated STEREO and Wind observations of a type III burst on 16 November 2006. (a) ST-A, (b) ST-B, and (c) Wind.

clearer. The data have been calibrated according to the procedure described in the previous section. The horizontal lines at higher frequencies correspond to terrestrial RFI, and could be removed by further data processing. The intensity scale is 10^{-15} – 10^{-20} $\text{Wm}^{-2}\text{Hz}^{-1}$. (1 solar flux unit = 10^{-22} $\text{Wm}^{-2}\text{Hz}^{-1}$) In previous studies, type III bursts have been observed with similar intensities [Fitzenreiter *et al.*, 1976; Reiner *et al.*, 1998]. It should be noted that although the same method has been used, each instrument has been calibrated independently. The close agreement between the two sets of observations indicates that the instruments are performing identically.

6.2. Comparison With Wind

[27] As a further test, we can compare the STEREO observations with similar observations made by the WAVES radio experiment on board the Wind spacecraft [Bougeret *et al.*, 1995]. The low-frequency receiver on Wind is generally well calibrated [Dulk *et al.*, 2001] and the data have been processed completely independently. Figure 5 shows the flux observed by the three spacecraft

during the Type III burst shown in Figure 4 between 200 kHz and 1 MHz, which corresponds to the WIND/WAVES low-frequency receiver range. The exact frequencies at which the instruments observe are slightly different; in particular WIND/WAVES alternates between two interleaved sets of frequencies. There is excellent agreement between the measurements. This is confirmed in Figure 6. Figure 6a compares the time series of radio flux at 0.925 MHz on STEREO A and B with the radio flux at 0.916 MHz on WIND. Figure 6b compares the STEREO 0.625 MHz and the WIND 0.624 MHz time series. In both cases the data are shown in SFU. There is a close agreement between the three independently calibrated sets of data.

7. Conclusions

[28] A prerequisite for quantitative studies of astrophysical and solar radio emission is an understanding of the antenna gain, so that the measured power can be converted into units of incident flux. This requires

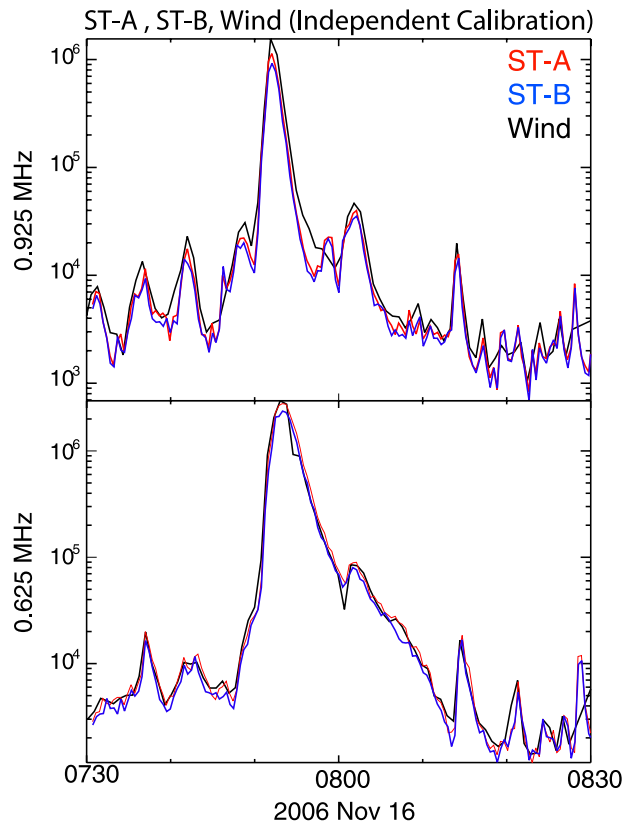


Figure 6. Comparison between calibrated STEREO and Wind observations of a type III burst at two sets of closely matched frequencies. (a) 0.925 MHz and (b) 0.625 MHz.

knowledge of (1) the antenna capacitance and effective length, (2) sources of noise, and (3) the antenna stray capacitance; therefore this calibration must be done in flight. Here we have examined the S/WAVES antenna system, using a theoretical model to determine the antenna capacitance and effective length, measuring sources of unwanted noise in the system, and determining the stray capacitance based on comparisons with the galactic nonthermal continuum.

[29] The calibration could be improved in future by developing a more precise model of the antenna capacitance. While the resulting model captures the resonance peak, the observed resonance peak is wider since the analytic expression does not include any stray resistivity (e.g., cables, preamp input) all of which act to broaden the resonance. A more complex model of the antenna capacitance could result in better reproduction of the resonant curve, and more accurate measurements above 10 MHz, albeit at the expense of ease of implementation. As mentioned in section 5, some small variations in noise levels, ascribed to temperature effects have also been observed. Once this is better understood, this may also result in further refinement of noise levels.

[30] Having quantified the appropriate free parameters, this information was used to determine the absolute flux profile of an illustrative type III solar radio burst observed on 16 November 2006 by both STEREO spacecraft. These results were also compared to simultaneous WIND observations of the same type III burst and were found to be in good agreement.

[31] **Acknowledgments.** For comments and discussion about different models of the galactic and extragalactic radio emission, the authors thank I. H. Cairns. This work was supported by NASA and CNES.

References

- Balanis, C. A. (2005), *Antenna Theory, Analysis Design*, 3rd ed., John Wiley, New York.
- Bale, S. D., et al. (2008), The electric antennas for the STEREO/WAVES experiment, *Space Sci. Rev.*, **136**, 529–547.
- Bougeret, J. L., et al. (1995), WAVES: The radio and plasma wave investigation on the Wind spacecraft, *Space Sci. Rev.*, **71**, 231–263.
- Bougeret, J. L., et al. (2008), S/waves: The radio and plasma wave investigation on the stereo mission, *Space Sci. Rev.*, **136**, 487–528.
- Cane, H. V. (1979), Spectra of the non-thermal radio radiation from the galactic polar regions, *Mon. Not. R. Astron. Soc.*, **189**, 465–478.
- Cecconi, B., et al. (2008), STEREO/WAVES goniopolarimetry, *Space Sci. Rev.*, **136**, 549–563.
- Dulk, G. A., W. C. Erickson, R. Manning, and J.-L. Bougeret (2001), Calibration of low-frequency radio telescopes using the galactic background radiation, *Astron. Astrophys.*, **365**, 294–300.
- Fitzenreiter, R. J., J. Fainberg, and R. B. Bundy (1976), Directivity of low frequency solar type III radio bursts, *Sol. Phys.*, **46**, 465–473.
- Hansen, R. C. (1981), Fundamental limitations in antennas, *Proc. IEEE*, **69**(2), 170–182.
- Kaiser, M. L., T. A. Kucera, J. M. Davila, O. C. St. Cyr, M. Guhathakurta, and E. Christian (2008), The STEREO mission: An introduction, *Space Sci. Rev.*, **136**, 5–16.
- Kellogg, P. J. (1981), Calculation and observation of thermal electrostatic noise in solar wind plasma, *Plasma Phys.*, **23**, 735–751.
- Manning, R. (2000), Instrumentation for space-based low-frequency radio astronomy, in *Radio Astronomy at Long Wavelengths*, *Geophys. Monogr. Ser.*, vol. 119, edited by R. G. Stone, K. Weiler, and J.-L. Bougeret, pp. 329–337, AGU, Washington, D. C.
- Manning, R., and G. A. Dulk (2001), The galactic background radiation from 0.2 to 13.8 MHz, *Astron. Astrophys.*, **372**, 663–666.
- Meyer-Vernet, N., and C. Perche (1989), Tool kit for antennae and thermal noise near the plasma frequency, *J. Geophys. Res.*, **94**(A3), 2405–2415.
- Novaco, J. C., and L. W. Brown (1978), Nonthermal galactic emission below 10 Megahertz, *Astrophys. J.*, **221**, 114–123.
- Oswald, T. H., W. Macher, H. O. Rucker, G. Fischer, U. Taubenschuss, J. L. Bougeret, A. Lecacheux, M. L. Kaiser, and K. Goetz (2009), Various methods of calibration of the STEREO/WAVES antennas, *Adv. Space Res.*, **43**, 355–364.
- Reiner, M. J., J. Fainberg, M. Kaiser, and R. G. Stone (1998), Type III radio source located by uylisses/wind triangulation, *J. Geophys. Res.*, **103**(A2), 1923–1931.
- Rucker, H. O., W. Macher, R. Manning, and H. P. Ladreiter (1996), Cassini model rheometry, *Radio Sci.*, **31**(6), 1299–1311.
- Zarka, P., B. Cecconi, and W. S. Kurth (2004), Jupiter's low-frequency radio spectrum from Cassini/Radio and Plasma Wave Science (RPWS) absolute flux density measurements, *J. Geophys. Res.*, **109**, A09S15, doi:10.1029/2003JA010260.
- S. D. Bale and J. P. Eastwood, Space Sciences Laboratory, University of California, 7 Gauss Way, Berkeley, CA 94720, USA. (eastwood@ssl.berkeley.edu)
- J.-L. Bougeret and M. Maksimovic, LESIA, Section Meudon, Observatoire de Paris, F-92195 Meudon CEDEX, France.
- K. Goetz, School of Physics and Astronomy, University of Minnesota, Minneapolis, MN 55455, USA.
- M. L. Kaiser, NASA Goddard Space Flight Center, Greenbelt, MD 20771, USA.
- I. Zouganelis, Laboratoire de Physique des Plasmas, UPMC, Ecole Polytechnique, CNRS, F-94107 Saint-Maur-des-Fossés, France.